On the role of helium metastable (2 3 S 1) measured by time resolved tunable diode laser spectroscopy in high current magnetron discharge

Abderzak El Farsy, Erwan Morel, Yoann Rozier, Ludovic de Poucques, Jacques Robert, Tiberiu Minea

Plasma Sources Science and Technology

On the role of helium metastable (2^3S_1) measured by time resolved tunable diode laser spectroscopy in high current magnetron discharge

On the role of helium metastable ($2\ ^3S_1$) measured by time resolved tunable diode laser spectroscopy in high current magnetron discharge

Abderzak El Farsy[1], Erwan Morel[1,2], Yoann Rozier[2], Ludovic de Poucques[3], Jacques Robert[1], Tiberiu Minea[1]

[1] Université Paris Saclay, CNRS, Laboratoire de Physique des Gaz et des Plasmas, (LPGP), - Orsay, France
[2] Supergrid Institute
[3] Université de Lorraine, CNRS, IJL, F-54000 Nancy, France

E-mail : erwanmorel@hotmail.fr; tiberiu.minea@universite-paris-saclay.fr

Abstract:

Tunable diode laser absorption spectroscopy is applied to measure the density and gas temperature of helium metastable (2^3S_1) *in the ionization region of magnetron discharge operated at very high current density (*$>10\ \mathrm{A.cm^{-2}}$*), which is achievable in helium at 10 Pa with molybdenum target. Those measurements were combined to electrical characterization of the current and the voltage at the magnetron cathode. The discharge current waveform is anti-correlated with the time-evolution of helium metastable (*He^m*) density showing that the main depletion process of* He^m *is its ionization. Counterintuitively, the higher the gas temperature the lower the discharge peak current. Gas rarefaction and gas recycling are discussed as major contributors for this phenomenon in very high current glow discharge.*

High power impulse magnetron sputtering (HIPIMS) is one of the very well established ionized physical vapor deposition (I-PVD) techniques, even if it has been developed significantly during the 21st century **[1].** HiPIMS uses a pulsed power supply delivering a huge peak power that exceeds the time-averaged power by typically two to three orders of magnitude. This implies the use of long off-time periods separating two consecutive pulses **[2]**. The peak power density, averaged over the target area, often exceeds $10^7\ W.m^{-2}$, aiming at the ionization of the sputtered atoms.

In the conventional magnetron discharges for thin film applications, the buffer gas (often Ar) pressure is usually below 2 Pa to improve the deposition rate **[3, 4]**. Recent works, carried out with pure Ne or Ar/Ne mixture **[5-7],** reported on the behavior of the discharge current, the gas recycling, and the final properties of deposited thin films. The literature has also shown specific interests for alternative gases like pure He **[8]**, He mixed with Ar **[9]** or H_2 **[10]**. More specifically, high current densities ($> 5\ \mathrm{A}.cm^{-2}$) **[11]** have been reported for pure helium, subject of the measurements presented in this paper**.**

Mainly, two methods have been explored for increasing the discharge current in glow mode: electrostatic confinement as in hollow cathodes **[12],** or specific $\vec{E} \times \vec{B}$ cathode designs **[13, 14]**. Both methods increase the electron residence time in the discharges. As a result, the gas ionization rate increases and therefore the discharge current.

Magnetically enhanced helium plasmas better respond to the former challenge (i.e., they generate the largest currents). So they are attractive for various applications such as Hall-effect thrusters **[15]**, plasma switches **[16],** and magnetron sputtering in specific conditions requiring light gases.

The HiPIMS current density is generally limited to $10\ \mathrm{A}\,.\,\mathrm{cm}^{-2}$ since beyond this limit the discharge evolves fast and irreversibly to an arc. Hence the current density typically remains below $5\ \mathrm{A}\,.\,\mathrm{cm}^{-2}$. Similar discharges in krypton and argon with niobium target give also a limited current density, below $3\ \mathrm{A}\,.\,\mathrm{cm}^{-2}$**[2]**. *Morel et al* have recently presented a new discharge glow regime with $\vec{E} \times \vec{B}$ configuration called Hyper Power Magnetron impulse discharge (HyPIM) **[17].** This discharge reached a current density of $31\ \mathrm{A}\,.\,\mathrm{cm}^{-2}$ without arc formation, for pulses up to 1 ms, using helium as gas and molybdenum as target material. This regime has been obtained by capping the applied voltage to 350 V together with the pre-ionization of the gas. The glow was stable over a range of pressure between 10 Pa - 30 Pa for very long pulses (1 ms) with a repetition rate below 5 Hz. The main application of this He discharge is the development of high-power switching devices where high current density is desirable and because the He ions have low sputtering efficiency compared to other gas (Ar, Ne ..) minimizing then the cathode erosion [18, 19].

In this work we take the advantage of high current density obtained using He gas to investigate the gas dynamic at the closest magnetron deposition condition (i.e. a pressure of 10 Pa) *via* the characterization of He metastable atoms (2^3S_1) evolution in HyPIM mode during a pulse of 50 µs at 100 Hz. The method used is the Time-Resolved Tunable Diode Laser Spectroscopy (TR-TDLAS) **[20].** Both parameters, density and temperature of helium metastable (He^m) are recorded. TR-TDLAS protocol is similar to the one reported for argon metastable atoms in HiPIMS mode **[20, 21]**. Still following also a similar approach as in the ionization region model **[22]**, the stepwise ionization *via* the metastable state appears to play a major role in He compared to HiPIMS in Ar **[21]** and even more important than in direct current (DC) magnetron discharge.

Our configuration uses a standard unbalanced magnetron cathode (GENCOA VT50, 2”, 850 G at the cathode surface) hosted in a stainless-steel chamber (35 cm diameter and 28 cm height). Before discharge ignition, the chamber was evacuated to a base pressure < 2 ×10^{-6} Pa by a water-cooled turbomolecular pump (Edwards EXT 501/ISO 160) combined with a dual-stage rotary pump (Pfeiffer DUO 10M). The base pressure was measured by a full range active Pirani compact cold cathode vacuum gauge (Pfeiffer PKR 361) and the helium (99.9995 % in purity) pressure as plasma gas was measured by a Baratron® capacitance manometer (MKS 627 BX). A throttle valve, installed between the vacuum chamber and the turbomolecular pump, was used to adjust the pressure to the desired level.

Square pulsed voltage was generated using an Ionautics pulsing unit (HiPSTER 10, 10 kW) fed by an Elektro-Automatik DC power supply (PS 9000 3U, 10 kW), up to -1 kV. Pulse frequency and duration were controlled by a Digital Delay Generator (Stanford Research system, model DG645). Voltage and current signals were recorded with an oscilloscope (Teledyne Lecroy, model WaveRunner 64Xi, 600 MHz bandwidth and a sampling frequency of 5 $Gs.s^{-1}$). The high voltage signal was acquired and reduced using a high voltage probe and a current probe incorporated in the pulsing unit. The pre-ionization DC source was managed with a Technix negative power supply (SR1KV-300W, operating up to 1.5 kV and 200 mA).

The sketch of the experimental setup for the TD-LAS technique is shown in **Fig. 1 (a)**. The laser beam emitted by the laser diode (Toptica DL 100, 40 mW maximum power) is divided into two beamlets by a splitter: the measurement beam (MB, 50% of the laser power) and the etalon beam (EB, 50%). The laser was accorded to probe the line $2^3S_1 \rightarrow 2\ ^3P_0$ [23]corresponding to λ_0= 1082.909 nm.

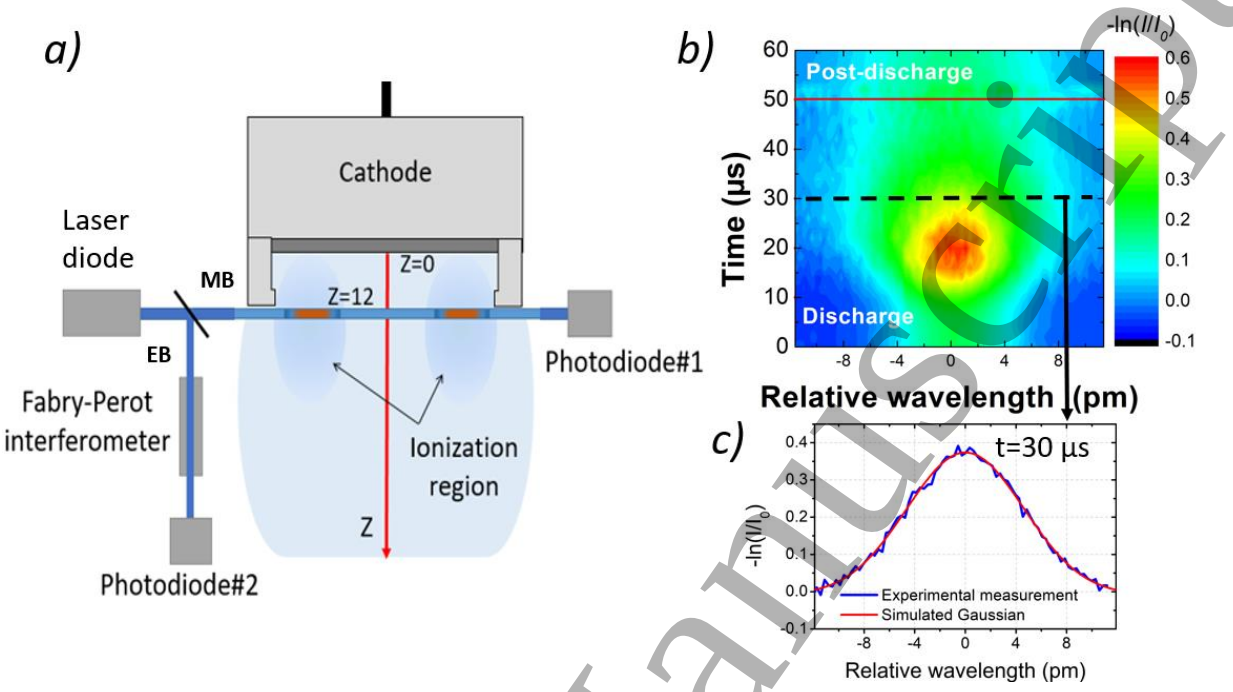

Fig. 1 : (a) Experimental setup; (b) Typical TD-LAS signal from a high current pulse measurement (z = 12 mm, p = 10 Pa, 400 A, P_{plasma}= 400W in He); (c) the fit of the absorption profile using Gaussian function (t=30 µs).

The MB probes the discharge parallel to the target surface and passes through the dense plasma in the so-called ionization region (IR) (z= 12 mm). The absorption length was assumed L=10 cm. The evolution of the laser beam intensities I_t and I_0, with and without plasma, respectively, is measured during the wavelength scan by a photodiode (InGaAs PIN detector ET-3000). A neutral filter (30% transmission of MB) limits the number of laser photons avoiding photodiode saturation. It was also verified that I_t was well proportional to I_0 (no saturation of the absorption transition **[24]**). The EB is directed to the Fabry-Perot interferometer, and the interference pattern gives the wavelength calibration.

Time-resolved measurement requires synchronizing the laser diode (LD) wavelength scan with the HyPIM pulses and the digital oscilloscope **[20]**. The LD is the slowest, with a ramp frequency of 0.5 Hz. Its TTL signal is the time reference for all devices (pulsing unit, current ramp for the laser diode, acquisition of the photodiode signal). During one LD ramp period, a fast function generator (Stanford Research system, model DG645) delivers 170 voltage pulses onto the cathode with frequency of 100 Hz. The laser wavelength is assumed constant during a single plasma discharge, for detailed description of this synchronization the reader is referred to **[20]**.

The discharge operates at a very high current (> 200 A), implying low frequency and short pulse width. Indeed, the regular cooling circuit can exhaust the excess calories (heat) only for very low duty cycle. In our case, the limit is 500 W, leading to a pulse duration to 50 µs but maximizing the pulse current as close as possible to the HyPIM mode.

The experimental procedure consists in isolating the TR-TDLAS signal for each discharge pulse and building a matrix $M(\lambda_i, t)$. **Fig. 1 (b)** shows this matrix, the wavelength λ_i(pm) is on the x-axis, and the

time (µs) is on the y-axis. One horizontal line corresponds to a Gaussian profile from which it is possible to extract the full width at half maximum ($\Delta\lambda_{\mathrm{FWHM}}$) (**Fig. 1 (c)**). Indeed, the Doppler broadening is the dominant process affecting the line width **[20]**. Therefore, it is possible to determine the metastable density Eq. (1) and the metastable temperature Eq. (2). The density is calculated as

$$[He^m](\mathrm{cm}^{-3}) = \frac{A_{max}}{L} \times \frac{2\varepsilon_0 m_e c^2}{e^2}\sqrt{\frac{\pi}{\ln 2}} \times \frac{\Delta\lambda_{\mathrm{FWHM}}}{f \times \lambda_0^2} = \frac{A_{max}}{L} \times \frac{\Delta\lambda_{\mathrm{FWHM}}}{8.25 \times 10^{-13} \times f \times \lambda_0^2} \quad (1)$$

where A_{max} is the maximal absorption (*i.e.* the absorption $\ln\left(\frac{I_0}{I}\right)$ at $\lambda=\lambda_0$), f the oscillator strength (6×10^{-2}) **[23]**, m_e and e the mass and the charge of electron, c the vacuum light velocity, ε_0 the vacuum permittivity, L is the effective absorbing path length and λ_0 is the absorption wavelength (1082.909 nm). The plasma is trapped by the magnetic field above the racetrack, thus the length L that must depend to the current density is assumed constant (L=8 cm). This assumption induces an error < 10% on He^m density. The temperature is given by the following formula

$$T(K) = \frac{mc^2 \Delta\lambda_{FWHM}^2}{8k_B \ln(2)\lambda_O^2} \quad (2)$$

where m is the mass of helium, c is the light speed and k_B is the Boltzmann constant.

Regarding the saturation of absorption transition, the saturation parameter S was calculated using the flowing formula [25]:

$$S = \frac{B_{ul}\,\rho}{R_l} \quad (3)$$

where B_{ul} the Einstein coefficient of the transition $2^3S_1 \rightarrow 2\,^3P_0$, ρ the spectral energy density and R_l the relaxation rate of the lower level. For laser operated at 18 mW power, 3 mm beam diameter, 100 MHz, gas temperature of 1000 K, neutral filter of 30% MB, entrance window of 70% MB, beam splitter of 50% MB, the saturation parameter is found to be 0.77 in which <1.

We compare the TR-TDLAS results for two peak currents (400 A and 230 A), obtained with a molybdenum target (50.8 mm diameter, 3 mm thick) in helium. They are expressed as current density (normalized to the whole target surface) to facilitate the comparison to other devices.

The first discharge (400 A) corresponds to $20\ \mathrm{A\,.\,cm^{-2}}$ or an (average) equivalent DC power of 400 W, while the second one (230 A) is $11.5\ \mathrm{A\,.\,cm^{-2}}$ for an equivalent DC power of 200 W. **Fig. 2(a)** and **(b)** shows the typical current-voltage waveforms for the two discharges. The pre-ionization corresponds to a weak DC discharge of about 37.5 W (U= 250 V and I= 150 mA). For the highest current density, the current reaches the peak value (400 A) 32 µs after the switch ON of the pulse and then decreases, ending the pulse at about half its maximum. The rise-time is slower at lower current density. The maximum (230 A) is reached after 37 µs but remains almost constant until the end of the pulse. **Fig. 2(c)** shows the corresponding time evolution of the helium metastable (He^m) density. The maxima for helium ($[He^m]_{max}$) rise before the peak current, 18 µs from the voltage pulse for 400 A and 26 µs for 230 A. Black dash lines mark the delay between the maxima for 400 A and red dash lines for 230 A. As

the $[He^m]_{max}$ precedes the peak current, it seems to indicate that the metastable state of helium participates further in the ionization process.

The time-evolution of the density of helium metastable state writes:

$$\frac{d[He^m]}{dt} = Source(t) - Loss(t) \quad (4)$$

As expected, this variation is positive (source > loss) at the beginning of the pulse, reaches an equilibrium (source = loss), and then it becomes negative (source < loss). For an HyPIM discharge, the main process producing helium metastable is Eq. (5), while the main loss process in the pulse writes as Eq. (6). In the case of helium, the experimental conditions are drastically changed with respect to the argon case (see **[22]** for details). The ionization level of helium is 24.6 eV, and its first metastable level (2^3S_1) is at 19.8 eV from the ground state. Therefore, the ionization from the metastable levels requires much less energetic electrons, about 5 eV (precisely higher than 4.8 eV).

$$Source: He + e^- \longrightarrow He^m + e^- \quad (5)$$

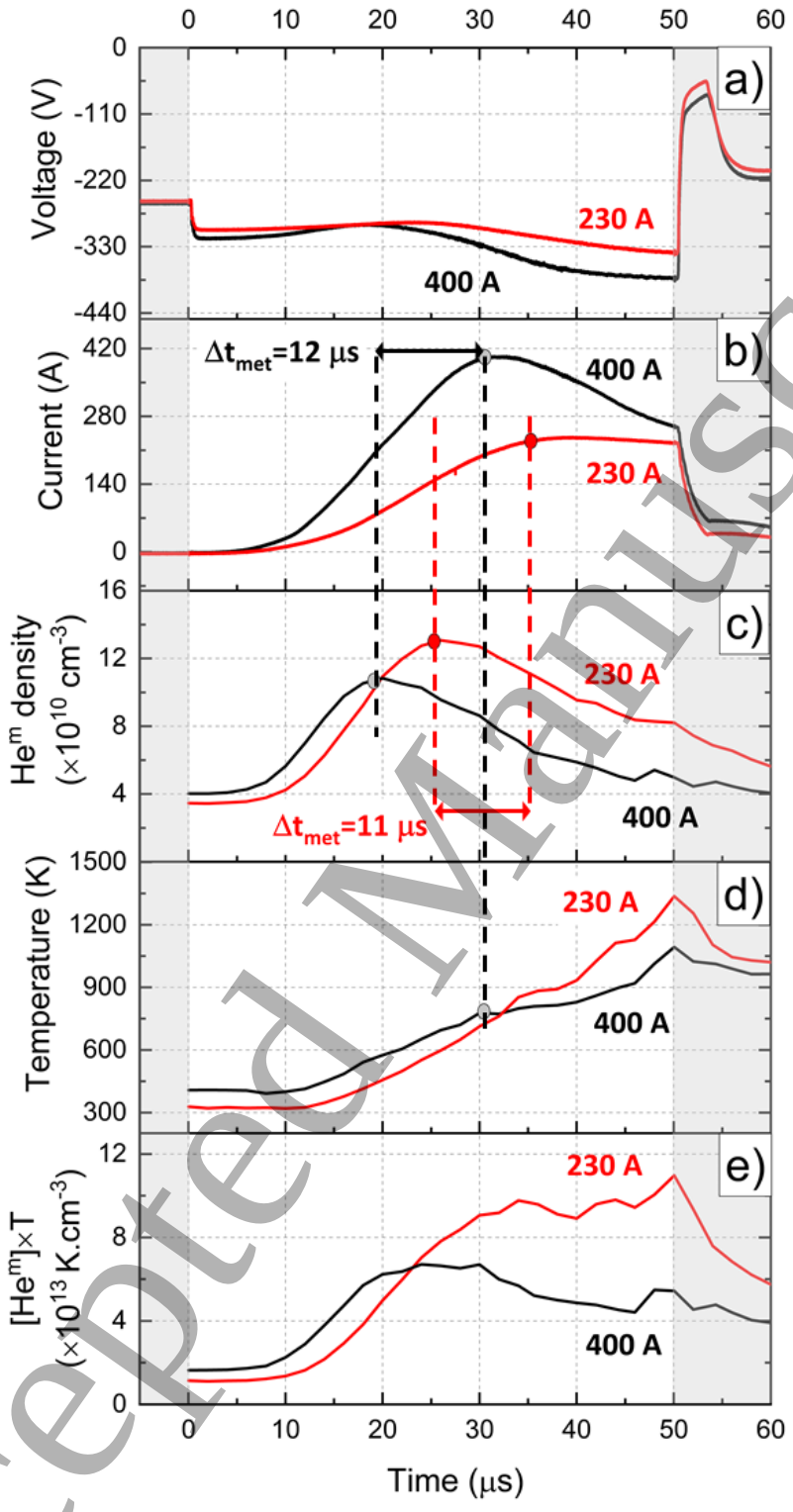

Fig. 2 : (a) Voltage; (b) Current; (c) metastable density, (d) He metastable temperature or the gas temperature; and (e) the product [He^m] × T as function of time. The white zone indicates the pulse, and the grey area represents the pre-ionization and afterglow. The error on He^m density is <10% and the error on the temperature is 40 K.

$$Loss: He^m + e^- \longrightarrow He^+ + 2e^- \quad (6)$$

Let us analyze panels **(b)** and **(c)** of **Fig. 2**. The interval time (Δt_{met}≈12 µs) between the I_{max} and $[He^m]_{max}$ is approximately constant for both studied cases. The fact that the density of He^m starts to rise simultaneously with the discharge current (~8 µs from the pulse ON) indicates the effective production and heating of the electrons. These energetic electrons lead to helium excitation (Eq. (5)) and its ionization by direct impact (Eq. (7)). However, the excitation energy threshold is smaller compared to ionization (19.8 versus 24.6 eV), and the metastable density increases faster. Once the maximum density $[He^m]_{max}$ is reached, the losses dominate over the production of He^m. Consequently, in the case of 400 A discharge, the He^m density decays continuously until the end of the pulse, and it is only 10% higher than the amount produced by the pre-ionization (the value at t=0). The two-stepwise ionization process can explain the decay, i.e., Eq. (6) follows immediately after Eq. (5). This mechanism is essential for the huge rise of the discharge current, and it sustains the discharge current all along the pulse.

$$Ionization: He + e^- \longrightarrow He^+ + 2e^- \quad (7)$$

The time evolution of the gas temperature is shown in **Fig. 2(d)**. A surprising behavior is observed in a time period of 18 µs before the pulse end, the gas temperature at 230 A is higher than 400A. Let us analyze panel (e) of **Fig. 2** which shows the time evolution of the relative pressure {P α $[He^m] \times T$} deduced from the product of gas density and the temperature. This pressure for the high current case (400 A) is 50 % lower than for 230 A at the end of the pulse. This phenomenon is well-known in the ionization region of HiPIMS discharge, and it is called the gas rarefaction **[1]**. It can be triggered by two phenomena, the first is related to gas recycling. Briefly, energetic He^+ ions bombarding the target get neutralized. As an inert gas, helium, like argon, does not create chemical bonds with the target material. They return to the gas phase as fast neutrals, hot (backscattered) or warm (in equilibrium with the surface temperature) in the majority. In both cases, their temperature is higher than the buffer gas, and via elastic collisions, they transfer a part of their energy, heating the gas. Further, these neutral atoms are again ionized near the cathode and finally 'recycled' to support the discharge current **[26]**. After several recycling loops, these neutral atoms with a high velocity push out of the ionization region a fraction of the buffer gas leading to its local rarefaction. In **[11]**, it has been demonstrated that gas recycling is present during a magnetron discharge operated with helium. It has also been demonstrated in a DC magnetron discharge operated in argon with a titanium target **[27]**, even if the effect is less important than in HiPIMS. The second mechanism leading to gas rarefaction is the sputter wind effect of ejected metal particles on the He gas. Metal particles, Mo in our case, are very heavy compared to the gas, can easily kick out the gas from the ionization region. He is a light gas, and the sputtering yield is very low, 0.022 **[28]** (for 320 eV). So, the presence of molybdenum in the discharge due to ionized helium is also low.

Nevertheless, for huge current (400 A), the effect of metal sputtered vapor on the gas can be significant. Notice that the self-sputtering coefficient is 20 higher (0.44 **[28]** for 320 eV) than the He sputtering coefficient, which may amplify enough metal density in the discharge to drive out the gas.

Finally, the buffer gas ionization effectiveness also contributes to the ground state rarefaction. In the hyper-power regime **[17],** the strong ionization with extreme discharge currents also induces gas rarefaction.

These three mechanisms, explained above, act together, reducing not only the local gas density (**Fig. 2(c)**) but also the pressure (**Fig. 2(e)**) at high current and explain why the gas temperature reaches a lower value at the end of the pulse for the discharge at 400 A (**Fig. 2(d)**). At moderate current (230 A), the rarefaction effect is contained, supported more by the gas heating rather than ionization.

In the light of these arguments, the current decay shown in **Fig. 2(b)** in the second part of the pulse is a consequence of the gas rarefaction. The negative slope observed t ~30 µs after the peak is higher at a huge current (400 A) and stays almost flat at a moderate current (230 A). Hence the rates of both direct excitation (Eq. (5)) and direct ionization (Eq. (7)) fall down.

To summarize, helium metastable atoms tracked by the TR-TDLAS technique unveiled the ionization mechanisms in a very high current regime, the so-called hyper-power impulse magnetron. It is characterized by a current density exceeding $10\ \mathrm{A}\,.\,\mathrm{cm}^{-2}$. These results demonstrate the major role played by the helium metastable state in the ionization process. Moreover, He^m appears a tracer for He ground state. The gas recycling and the two stepwise ionizations play a major role to reach a very high current density ($20\ \mathrm{A}\,.\,\mathrm{cm}^{-2}$). The rarefaction strongly limits the current rise after the peak, especially for higher currents, where it can exceed 50 %. This rarefaction plays a key role in decreasing the current and prevents from maintaining the current at a high level. These measurements unravel the insights towards understanding HyPIM discharges and the difficulties in preserving high current density magnetron operation.

Acknowledgment

This work was supported by a grant from the French National Research Agency (ANR) as part of the "Investissement d'Avenir" Program (ANE-ITE-002-01).

Data Availability

The data that support the findings of this study are available from the corresponding author upon reasonable request.

References

[1] D. Lundin, J. T. Gudmundsson, and T. Minea, *High Power Impulse Magnetron Sputtering: Fundamentals, Technologies, Challenges and Applications*. Elsevier, 2019.

[2] A. Anders, "Discharge physics of high power impulse magnetron sputtering," *Surface and Coatings Technology*, vol. 205, pp. S1 – S9, 2011, pSE 2010 Special Issue.

[3] Andre Anders, "A review comparing cathodic arcs and high power impulse magnetron sputtering (HiPIMS)," *Surface and Coatings Technology*, vol. 257, pp. 308 – 325, 2014, 25 years of TiAlN hard coatings in research and industry.

[4] J. T. Gudmundsson, N. Brenning, D. Lundin, and U. Helmersson, "High power impulse magnetron sputtering discharge," *Journal of Vacuum Science & Technology A*, vol. 30, no. 3, p. 030801, 2012.

[5] A. Aijaz, K. Sarakinos, D. Lundin, N. Brenning, and U. Helmersson, "A strategy for increased carbon ionization in magnetron sputtering discharges," *Diamond and related materials*, vol. 23, pp. 1–4, 2012.

[6] N. P. Poluektov, I. Usatov, and M. Kladov, "Investigation of carbon ionization in hipims discharge with a hollow cathode magnetron," *Plasma Sources Science and Technology*, 2021.

[7] F. Cardoso, F. Ferreira, A. Cavaleiro, and A. Ramalho, "Performance of diamond-like carbon coatings (produced by the innovative ne-hipims technology) under different lubrication regimes," *Wear*, p. 203775, 2021.

[8] V. Tiron, C. Andrei, A. V. Nastuta, G. B. Rusu, C. Vitelaru, and G. Popa, "Carbon and tungsten sputtering in a helium magnetron discharge," *IEEE transactions on plasma science*, vol. 37, no. 8, pp. 1581–1585, 2009.

[9] S. Krat, E. Fefelova, A. Prishvitsyn, Y. Vasina, Z. Harutyunyan, Y. Gasparyan, and A. Pisarev, "Helium accumulation in tungsten layers deposited in Ar-He magnetron discharge," vol. 1686, no. 1, p. 012020, 2020.

[10] D. V. Mozgrin, I. K. Fetisov, and G. V. Khodachenko, "High-current low-pressure quasi-stationary discharge in a magnetic field: Experimental research," 1995.

[11] E. Morel, Y. Rozier, C. Ballages, R. Bazinette, T. Forchard, C. Creusot, A. Girodet, and T. Minea, "Behavior of high current density pulsed magnetron discharge with a graphite target," *Plasma Sources Science and Technology*, vol. 30, no. 12, p. 125001, dec 2021.

[12] V. Kolobov and A. Metel, "Glow discharges with electrostatic confinement of fast electrons," *Journal of Physics D: Applied Physics*, vol. 48, no. 23, p. 233001, 2015.

[13] A. V. Kaziev, D. V. Kolodko, A. V. Tumarkin, M. M. Kharkov, and T. V. Stepanova, "Ion energy distributions at a cathode in a non-sputtering magnetron discharge," vol. 2, pp. 1–3, Sep. 2016.

[14] D. M. Goebel, "Cold-cathode, pulsed-power plasma discharge switch," *Review of Scientific Instruments*, vol. 67, no. 9, pp. 3136–3148, 1996.

[15] D. M. Goebel and I. Katz, *Fundamentals of electric propulsion: ion and Hall thrusters*. John Wiley & Sons, vol. 1.2008

[16] R. W. Schumacher and R. J. Harvey, "Modulator switch with low voltage control," Jun. 24 1986, US Patent 4,596,945.

[17] E. Morel, Y. Rozier, and T. Minea, "Hyper power impulse magnetron–hypim–glow discharge," *EPL (Europhysics Letters)*, 2022.

[18] D. Levko, R. R. Upadhyay, and L. L. Raja, "Operating modes of a magnetized direct-current discharge in helium at pressures 10 pa," *Journal of Applied Physics*, vol. 129, no. 18, p. 183307, 2021.

[19] C. A. Allen, W. N. G. Hitchon, S. C. Aceto, D. J. Smith, T. J. Sommerer, J. F. Trotter, and J. E. Lawler, "Erosion rates of diffuse and constricted magnetron discharges in helium over aluminium, gallium, molybdenum, and tantalum," *Journal of Physics D: Applied Physics*, vol. 52, no. 43, p. 435203, 2019.

[20] C. Vitelaru, D. Lundin, G. Stancu, N. Brenning, J. Bretagne, and T. Minea, "Argon metastables in hipims: time-resolved tunable diode-laser diagnostics," *Plasma Sources Science and Technology*, vol. 21, no. 2, p. 025010, 2012.

[21] J. T. Gudmundsson, D. Lundin, G. Stancu, N. Brenning, and T. Minea, "Are the argon metastables important in high power impulse magnetron sputtering discharges?" *Physics of Plasmas*, vol. 22, no. 11, p. 113508, 2015.

[22] G. Stancu, N. Brenning, C. Vitelaru, D. Lundin, and T. Minea, "Argon metastables in hipims: validation of the ionization region model by direct comparison to time resolved tunable diode-laser diagnostics," *Plasma Sources Science and Technology*, vol. 24, no. 4, p. 045011, 2015.

[23] J. Winter, J. S. Sousa, N. Sadeghi, A. Schmidt-Bleker, S. Reuter, and V. Puech, "The spatio-temporal distribution of he (23s1) metastable atoms in a mhz-driven helium plasma jet is influenced by the oxygen/nitrogen ratio of the surrounding atmosphere," *Plasma Sources Science and Technology*, vol. 24, no. 2, p. 025015, 2015.

[24] N. Sadeghi, "Saturation optique et autres pièges en spectroscopie laser," 2004.

[25] N. Sadeghi, "Practical aspects of molecular spectroscopy in plasmas 6. molecular spectroscopy techniques applied for processing plasma diagnostics," *Journal of Plasma and Fusion Research*, vol. 80, no. 9, pp. 767–776, 2004.

[26] N. Brenning, J. T. Gudmundsson, M. A. Raadu, T. J. Petty, T. Minea, and D. Lundin, "A unified treatment of self-sputtering, process gas recycling, and runaway for high power impulse sputtering magnetrons," *Plasma Sources Science and Technology*, vol. 26, no. 12, p. 125003, nov 2017.

[27] A. Revel, A. El Farsy, L. de Poucques, J. Robert, and T. Minea, "Transition from ballistic to thermalized transport of metal-sputtered species in a dc magnetron," *Plasma Sources Science and Technology*, vol. 30, no. 12, p. 125005, 2021.

[28] N. Matsunami, Y. Yamamura, Y. Itikawa, N. Itoh, and Y. Kazumata, "Energy dependence of sputtering yields of monatomic solids," Nagoya Univ.(Japan). Inst. of Plasma Physics, Tech. Rep., 1980.